Photopyroelectric thin-film instrumentation and impulse-response detection. Part III: Performance and signal recovery techniques

Joan F. Power and Andreas Mandelis

Photoacoustic and Photothermal Sciences Laboratory, Department of Mechanical Engineering, University of Toronto, Toronto, Ontario M5S 1A4, Canada

(Received 7 May 1987; accepted for publication 21 July 1987)

Frequency-modulation time-delay spectrometry (FM-TDS) was compared with stochastic excitation in photopyroelectric measurements on thin solid samples. These methods involve broadband signal excitation with simultaneous detection of all frequency components within the response bandwidth of the photothermal system. Fast signal recovery was achieved by FFT methods. Both FM-TDS and wideband random-noise excitation were found to yield high-quality, band-limited impulse-response information. Random noise measurements were found to be much less susceptible to distortions and nonlinearities in the excitation wave train. FM-TDS showed superior coherence and signal-to-noise ratio (SNR) to random methods. The results of this work demonstrate a photopyroelectric effect spectrometer capable of yielding fast, time-resolved information equivalent to the response of a pulsed laser, with low peak power. This important feature shows excellent potential for nondestructive thickness, thermal diffusivity, and thermal conductivity measurements on materials which are susceptible to optical damage.

INTRODUCTION

The technique of frequency-modulation time-delay spectrometry (FM-TDS)[1–4] has been applied to the photopyroelectric (P^2E) measurement of the thermal properties of thin solid samples, as described in Part II of this work.[5] The superior performance characteristics of FM-TDS with respect to dynamic range and noise rejection[1–4] enable the fast recovery of high-resolution impulse-response information from photothermal systems, with dramatic decreases in measurement time and improved data resolution.[4,6,7] The impulse-response information available from broadband-modulated cw techniques in general is of special interest in photopyroelectric spectroscopy[8–11] (P^2ES) because time-resolved information, made available from a low-power, highly stable cw intensity-modulated source, is equivalent to the response obtained from a high-power pulsed laser, averaged over many pulses.[12] The ease of interpretation of impulse response information is yet another advantage because the time-delay-domain response of a system is directly related to the transit velocity of thermal signals through the sample material,[5,10,11] and hence, is capable of directly yielding thermal diffusivity or thickness measurements. The high-peak-power requirement of pulsed laser photoacoustic and photothermal methods in general is prohibitive[10,13] in the study of delicate or photosensitive materials, with low-power cw broadband-modulation methods providing an attractive, high-performance alternative.

In Part II of this work, we reported the implementation of a frequency-modulation time-delay photopyroelectric spectrometer. In this work, our objective has been to examine the performance of our instrument using two separate cw broadband-modulation methods. Specifically, we have compared the performance of (a) a stochastic excitation method using wideband random noise and (b) the minimum phase excitation method of FM-TDS, which has demonstrated a record of superior coherence and noise rejection in both the photothermal[6,7] and acoustical field.[1] The purpose of the present work is to demonstrate the performance and speed improvements offered by FM-TDS in photopyroelectric measurements, and compare its performance with the classical random excitation methods.

I. THEORETICAL: SPECTRAL COMPUTATIONS AND CRITERIA OF UNIFORMITY

The theoretical application of FM-TDS to photothermal systems was originally developed by Mandelis.[4] In this section, we briefly review this theory and discuss aspects of particular relevance to the present experiments.

In cw broadband-modulation experiments, the general avenue for signal recovery is correlation and spectral analysis.[1,2,14] The use of an FFT signal analyzer such as the HP 3562A enables the recovery of all correlation functions by inverse transformation of averaged spectral density functions. This is made feasible by means of the Weiner–Khinchine relations[14] in which successive Fourier transforms of the input $X(f)$ and output $Y(f)$ are averaged over a measurement period T:

$$G_{xx}(f) = \lim_{T\to\infty} (1/T)\langle X^*(f)X(f)\rangle, \tag{1}$$

$$G_{yy}(f) = \lim_{T\to\infty} (1/T)\langle Y^*(f)Y(f)\rangle, \tag{2}$$

$$G_{xy}(f) = \lim_{T\to\infty} (1/T)\langle X^*(f)Y(f)\rangle, \tag{3}$$

for the autospectra of the input and output, $G_{xx}(f)$ and $G_{yy}(f)$, respectively, and for the cross spectrum, $G_{xy}(f)$.

The cross and autocorrelation functions, $R_{xy}(\tau)$ and

 0034-6748/87/112033-11$01.30 © 1987 American Institute of Physics

Downloaded 18 Jul 2008 to 128.100.49.17. Redistribution subject to AIP license or copyright; see http://rsi.aip.org/rsi/copyright.jsp

$R_{xx}(\tau)$, are recovered by inverse transformation of Eqs. (1)–(3) to give the appropriate correlation functions:

$$R_{xx}(\tau) = \int_0^\infty e^{2\pi j f\tau} G_{xx}(f)\,df, \tag{4}$$

$$R_{yy}(\tau) = \int_0^\infty e^{2\pi j f\tau} G_{yy}(f)\,df, \tag{5}$$

$$R_{xy}(\tau) = \int_0^\infty e^{2\pi j f\tau} G_{xy}(f)\,df. \tag{6}$$

Similarly, frequency-response (transfer function) data are directly recovered from the spectral density functions as[14]

$$H(f) = G_{xy}(f)/G_{xx}(f) = |H(f)|e^{j\phi(f)} \tag{7}$$

from cross-spectral density data and

$$|H(f)| = [G_{yy}(f)/G_{xx}(f)]^{1/2} \tag{8}$$

from autospectral data.

The strategy of broadband-modulated cw techniques, in general, is to excite the photothermal system with $G_{xx}(f) = 1$. Equivalently, the input autocorrelation function must satisfy $R_{xx}(\tau) \sim \delta(\tau)$ on the time scale of the experiment. This has the consequences

$$H(f) \sim G_{xy}(f), \tag{9}$$

and

$$h(\tau) \sim Rh(\tau) * \delta(\tau) \sim h(\tau) * R_{xx}(\tau) \sim R_{xy}(\tau).$$

Thus, the flat input autospectrum yields the equivalent of impulse excitation in the time-delay domain through both impulse response and cross-correlation functions.

It is relatively easy to visualize the application of these correlation techniques in experiments which use stochastic excitation. By using random noise of sufficiently wide bandwidth as the excitation waveform, the flatness of the input autospectrum is maintained. By contrast, it is important to verify that the condition $G_{xx}(f) = 1$ is valid for excitation by deterministic signals. In particular, the linear sine sweeps used for signal excitation in FM-TDS techniques possess flat autospectra only in the limit of sufficiently long sweep times. The consequences of any spectral approximations impact directly on the quality of the spectral functions and frequency-response information obtained.

In FM-TDS measurement, the form of the excitation waveform $x(t)$ is a linear cosine sweep:

$$x(t) = \begin{cases} A\cos(\pi S t^2 + 2\pi f_a t + \theta_a), & 0 \leqslant t \leqslant T, \\ 0 & t > T, \end{cases} \tag{10}$$

where A is the amplitude of the sweep function, S is the sweep rate (a constant in this case), f_a is the initial frequency in the sweep, and θ_a is the initial phase.

These quantities are easily understood with reference to the schematic of Fig. 1. The excitation consists of a cosine waveform with a time-varying frequency $f_i = f_a + St$, where f_i is the "instantaneous" frequency. Because it is time varying, is not frequency in the Fourier sense. The sweep has a duration T and frequency span (modulation bandwidth) $\Delta f = f_b - f_a$, and is assumed to repeat itself with period T.

For the conditions of the present experiments, $f_a = 0$ and $\theta_a = 0$. $A = 1$ arbitrarily so that

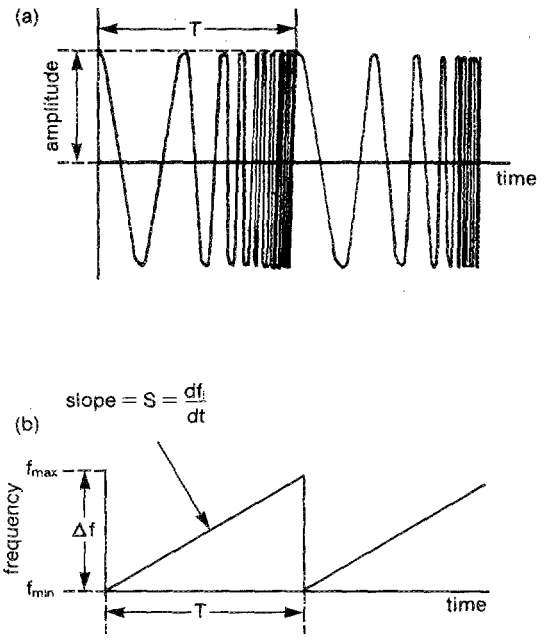

FIG. 1. Schematic representation of linear frequency sweep concepts (a) amplitude–time profile, (b) frequency–time profile corresponding to (a).

$$x(t) = \cos \pi S t^2 = \tfrac{1}{2}(e^{j\pi S t^2} + e^{-j\pi S t^2}) = x_+(t) + x_-(t). \tag{11}$$

Therefore, $x(t)$ is the sum of two counter-rotating phasors: $x_+(t) = e^{j\pi S t^2}$ and $x_-(t) = e^{-j\pi S t^2}$ with the polarization of each component indicated by (+) and (−).

For a single linear sweep of finite duration T, the one-sided Fourier transform of Eq. (11) may be computed directly:

$$X_\pm(\omega) = \int_0^T e^{-j\omega t} e^{\pm j\pi S t^2}\,dt,$$

$$X_\pm(\omega) = \frac{e^{\mp j\omega^2/8\pi S}}{2S^{1/2}} \times \left[Ci\left(2S^{1/2}T \mp \frac{f}{2S^{1/2}}\right) \pm Ci\left(\frac{f}{S^{1/2}}\right) \pm jSi\left(2S^{1/2}T \mp \frac{f}{S^{1/2}}\right) + Si\left(\frac{f}{S^{1/2}}\right)\right], \tag{12}$$

where

$$Ci(x) = \int_0^x \cos\left(\frac{\pi}{2}u^2\right)du,$$

$$Si(x) = \int_0^x \sin\left(\frac{\pi}{2}u^2\right)du.$$

This expression is useful because it enables the frequency content of a single sweep to be determined analytically. The autocorrelation function for the sweep, $R_{xx}(\tau)$ is computed by definition[2,14]:

$$R_{xx}(\tau) = \frac{1}{T}\int_{-\infty}^{\infty} x^*(t)x(t+\tau)dt. \tag{13}$$

For the linear sweeps described by Eq. (10),

Downloaded 18 Jul 2008 to 128.100.49.17. Redistribution subject to AIP license or copyright; see http://rsi.aip.org/rsi/copyright.jsp

$$R_{xx}(\tau) = (1/T)\left[R_{x_+x_+}(\tau) + R_{x_-x_+}(\tau) + R_{x_+x_-}(\tau) + R_{x_-x_-}(\tau)\right], \tag{14}$$

where[2]

$$R_{x_+x_+}(\tau) + R_{x_-x_-}(\tau) = \frac{1}{4}\frac{T-|\tau|}{T}\left(\frac{(e^{j2\pi S\tau(T-|\tau|)}-1)}{j2\pi S\tau(T-|\tau|)} - \frac{(e^{-j2\pi S\tau(T-|\tau|)}-1)}{j2\pi S\tau(T-|\tau|)}\right) \tag{15}$$

and

$$R_{x_+x_-}(\tau) + R_{x_-x_+}(\tau) = \frac{1}{2T}\int_{|\tau/2|}^{T-|\tau/2|}\cos\left[2\pi S\left(t^2+\frac{\tau^2}{4}\right)\right]dt. \tag{16}$$

For large T, Eq. (16) approximates to $1/[8\sqrt{(\Delta f)T}]$ so that its contribution is suppressed with long sweep times T and wide modulation bandwidths Δf.

It is possible to attain the condition $R_{xx}(\tau)\approx\delta(\tau)$ if the cross terms in Eq. (16) are zero so that

$$R_{xx}(\tau)\approx R_{x_+x_+}(\tau) + R_{x_-x_-}(\tau).$$

Even with the cross terms suppressed, it is still not obvious why and when $R_{x_+x_+}(\tau) + R_{x_-x_-}(\tau)\approx\delta(\tau)$. This may be clarified by considering the desired condition $G_{xx}(f) = 1$. Ideally, this condition is only met as $\Delta f\to\infty$. Infinite modulation bandwidth is neither achievable nor actually required in practice as long as the output response of the photothermal system, $Y(f)\sim 0$ for $f > f_{\max}$.

For long enough sweep times $T \gg |\tau|$, the "autopolarized" terms in Eq. (11) become

$$R_{x_+x_+}(\tau) + R_{x_-x_-}(\tau) = \frac{1}{4}\frac{e^{j2\pi(\Delta f)\tau}-1}{2\pi jS\tau T} - \frac{1}{4}\frac{e^{-j2\pi\Delta f\tau}-1}{2\pi jS\tau T} = \sin(2\pi\Delta f\tau)/4\pi\Delta f\tau. \tag{17}$$

This result has the identical form predicted for the real part of the inverse Fourier transform of the idealized square frequency window depicted in Fig. 2. As the modulation bandwidth Δf approaches very large values, the real part of $R_{xx}(\tau)$ approaches the Dirac delta function $\delta(\tau)$.

The imaginary part of the time-domain expression is shown in Figs. 2(b) and 2(c), however, it constitutes redundant information, since it is readily obtainable from the real part by Hilbert transformation.[1]

The form of the input autocorrelation function is thus demonstrated to be mathematically equivalent to a Dirac delta function provided the sweep time is long. If the sweep time is insufficiently long, i.e., $T \leqslant 1/2\pi S\tau$, the approximation to the Dirac delta function, which is recovered by standard correlation techniques, no longer applies.

II. EXPERIMENTAL

The FM-TDS photopyroelectric-effect spectrometer used in this work has been described in detail in Part II of this work. The spectrometer was equipped with a fast detector element consisting of a thin film (28-μm thick) of polyvinylidene difluoride (PVDF) (Penwalt Corp.) and a buffer/preamplifier (Comlinear CLC-B-600; 3-pF parallel 3-MΩ input impedance; 600-MHz bandwidth). The buffer signal was applied as $y(t)$ to the HP 3562A dynamic signal analyzer used in our experiments. All excitation waveforms studied in this work were supplied by the internal source of the HP

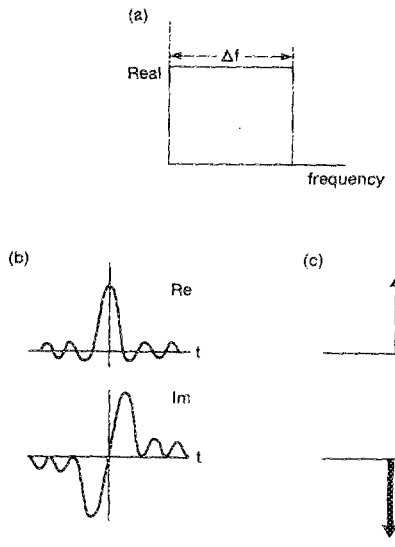

FIG. 2. Frequency–time schematics showing (a) idealized square frequency window $u(f-f_a)$ and (b) its Fourier transform (IFT); (c) Fourier transform of (a) in the limit $f_{\max}\to\infty$; $d(t)$ stands for the doublet symbol (i.e., the imaginary component of the inverse Fourier transform of the infinitely broadband frequency window).

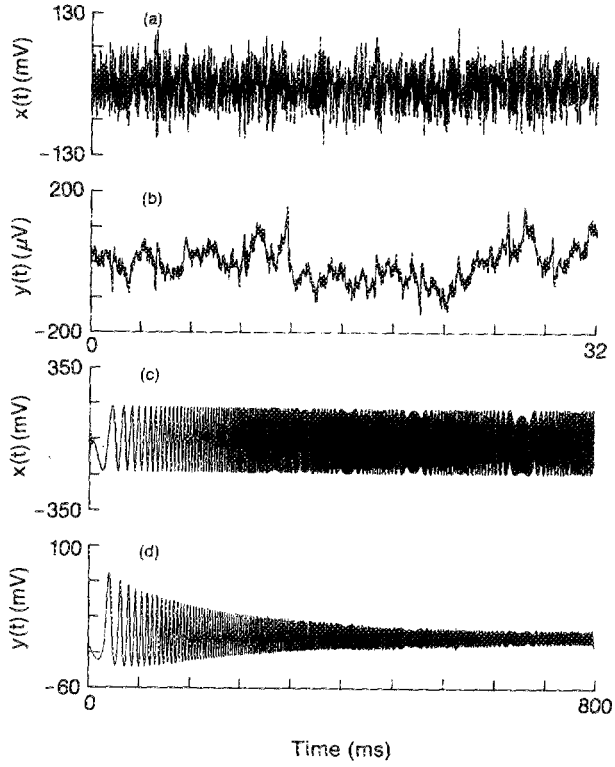

FIG. 3. Comparison of random noise [(a) and (b)] and FM-TDS [(c) and (d)] excitation waveform for thin-film PVDF detector: (a) $x(t)$ and (b) $y(t)$ recorded with $\Delta f = 0$–25 kHz; (c) $x(t)$ and (d) $y(t)$ recorded with $\Delta f = 0$–1 kHz.

Downloaded 18 Jul 2008 to 128.100.49.17. Redistribution subject to AIP license or copyright; see http://rsi.aip.org/rsi/copyright.jsp

3562A. The frequency spans of these waveforms, Δf, were user adjustable up to 100 kHz. The range of frequency spans used in this work was from 0–25 kHz (upper limit) to 0–25 Hz (lower limit) depending on the thickness of the samples in contact with the PVDF film. Random noise and FM-TDS measurements were made in the HP 3562A's linear resolution mode in which the sweep time T and the frequency span Δf were interdependent and related by the expression $(\Delta f)T = 800$.[15] The excitation waveforms were applied to the input of an ISOMET 1201E acousto-optic modulator driver. The modulator was used to time vary the intensity of a 488-nm Ar^+ laser beam which generated thermal waves in the sample by surface light absorption.[6,7] The modulation depth was optimized by applying a 400-mV peak-to-peak signal to the modulator driver. The output of the HP 3562A internal source supplied the $x(t)$ waveform to the analyzer.

Time-and-frequency-domain averaging was carried out by the HP 3562A with the choice of the number of averages made depending on the user-selected frequency span Δf. Time-domain averaging was the main factor in controlling the SNR in these experiments as discussed in the next section.

Uniform windowing of all data records was used, with the low-frequency cutoff of the input signals set below 1 Hz by the bandpass of the ac coupling networks at the input to the HP 3562A. Figure 3 shows typical examples of $x(t)$ and $y(t)$ input waveforms for the PVDF detector as recorded by our FFT analysis system.

III. RESULTS AND DISCUSSION

A. Time-delay-domain system performance

Our photopyroelectric system was characterized in this work by studying the response of the fast, thin-film pyroelectric detector in contact with varying thicknesses of quartz. The front surface of the samples was coated with a thin layer of ink to serve as a blackbody. Details on the preparation of these samples are reported in Part II of this work.

All frequency and time-delay-domain functions reported in this work were recovered by calculations carried out with an HP 3562A dynamic (FFT) signal analyzer. Impulse-response information was obtained by inverse transformations of the measured frequency response:

$$h(\tau) = \int_0^{f_{\max}} e^{+j2\pi f\tau} H(f)\,df, \tag{18}$$

where $H(f)$ is defined in Eq. (7) and $f_{\max}$ is the maximum experimental sweep frequency.

The one-sided spectral density functions, in turn, were computed from the Weiner–Khinchine relations [Eqs. (1)–(3)], with arithmetic averaging of the products of all Fourier transforms $X(f)$ and $Y(f)$. All correlation functions were recovered by the inverse Fourier transformation of the corresponding spectral density functions.

Because broadband (cw) modulation methods may be generally categorized into stochastic and deterministic types, we have chosen to compare random noise excitation, to which standard correlation analysis rigorously applies,[14] with the swept wave excitation characteristic of FM-TDS,

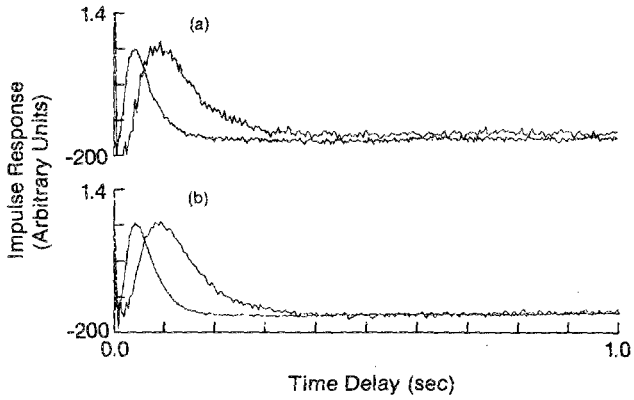

FIG. 4. Comparative impulse response profiles for samples of quartz: (a) random noise recordings (b) FM-TDS recordings. Sample thicknesses were 400 μm (early peak) and 600 μm (later peak). Time-delay parameters: *random noise*: $\tau_d = 42.97$ ms (400 μm) and 85.94 ms (600 μm); Peak widths: $\Delta\tau_d = 35.2$ ms (400 μm) and 78.16 ms (600 μm); *FM-TDS results*: $\tau_d = 42.97$ ms (400 μm) and 85.94 ms (600 μm); Peak widths: $\Delta\tau_d = 37.11$ ms (400 μm) and 78.16 ms (600 μm). $\Delta f = 200$ Hz. Both magnitudes were normalized to a maximum of 1 (arbitrary units).

for which it applies in the limit of sufficiently long sweep time.[1,2]

The primary information of interest in time delay P^2E experiments is extracted from the impulse response $h(\tau)$ of the photothermal system. Figure 4 shows a series of typical impulse profiles obtained from our instrument with different layers of quartz in contact with the PVDF detector. As the sample thickness increases, the impulse response maximum shifts to longer time delays τ_d because the transit time of the thermal energy through the sample increases approximately as the square of the sample thickness.[5] In addition, the peak intensity decreases and the peak width increases proportionately with thickness. The variation of these factors is described quantitatively in Part I of this work by means of the appropriate Green's function model.[16]

The impulse responses of Figs. 4(a) and 4(b) were recorded using wideband random noise and FM-TDS swept wave excitation, respectively. These results show that congruent responses are obtained in the time-delay domain with both types of excitation resulting in essentially identical peak delays and peak widths to within experimental error. Evidence that both of these sets of responses corresponded to the "true" $h(\tau)$ for the sample/pyroelectric system, was demonstrated in Parts I and II of this work, which showed direct agreement between the experimental and theoretical time-delay-domain $h(\tau)$ profiles.[5,16]

The impulse response profiles of Fig. 4 exhibit a spike and a corresponding droop in the baseline prior to the arrival of the thermal pulse transmitted by the sample. Tests verified that this feature was due to the direct synchronous excitation of the PVDF detector film due to light leakage through the blackbody layer, and in some cases, due to light scattered from the front surface of the sample onto the detector. This feature is well resolved from the signals obtained from the thicker samples studied in this work ($l > 390\,\mu$m). Thinner samples yield signals which are not as well resolved, temporally, but for the thinner samples, the signal intensity

Downloaded 18 Jul 2008 to 128.100.49.17. Redistribution subject to AIP license or copyright; see http://rsi.aip.org/rsi/copyright.jsp

is much greater relative to the stray PVDF response, since the intensity of the sample peak is governed by diffusional processes, and thus it increases rapidly with decreasing sample thickness. In both cases, the peak delays may be easily resolved from the PVDF signal. The $\Delta\tau_d$ widths for the trailing edge of the sample response are not significantly affected and agree well with the theoretical predictions of Part II of this work.[5]

An important criterion indicating the success of the wideband strategy is the agreement between the impulse response $h(\tau)$ and the cross-correlation function $R_{xy}(\tau)$ for the measurement. Figure 5 shows the agreement obtained between $h(\tau)$ and $R_{xy}(\tau)$ for (a) wideband random noise and (b) FM-TDS swept wave excitation. The sample was a thin piece of 400-μm quartz.

A detailed comparison of $R_{xy}(\tau)$ and $h(\tau)$ for both methods shows excellent agreement between the two functions for recovery of peak delay information. The random noise measurements, in particular, yielded time-delay-domain functions which superimposed to within experimental error. The FM-TDS data, on the other hand, showed good agreement between peak delays, but a systematic variance in the peak widths due to distortions in the trailing edge of $R_{xy}(\tau)$. The cross-correlation peaks were actually narrower than the impulse response peaks. This feature, discussed in Sec. IV, was found to be due to power losses at the edges of the $G_{xx}(f)$ modulation band recovered from the FM-TDS sweep. Because the analyzer recovers frequency-response information from the ratio $G_{xy}(f)/G_{xx}(f)$ and $R_{xy}(\tau)$ was recovered by inverse Fourier transformation of $G_{xy}(f)$, any differences between $h(\tau)$ and $R_{xy}(\tau)$ are traceable to nonuniformities in $G_{xx}(f)$. Consequently, the degree of agreement between $R_{xy}(\tau)$ and $h(\tau)$ is an indirect indicator of the validity of the autospectral flatness condition $G_{xx}(f) = 1$, and a means of evaluating the relative importance of various spectral nonuniformities on the time-delay-domain functions.

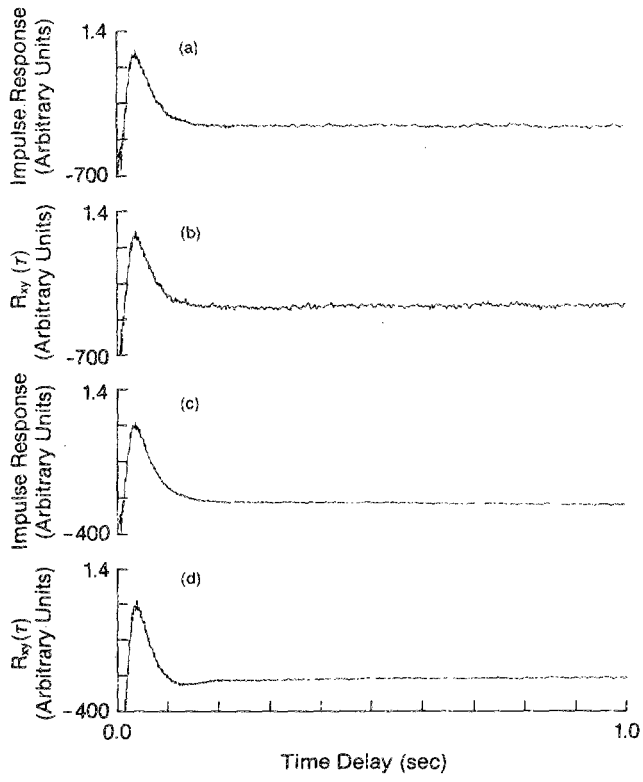

FIG. 5. Impulse response $h(\tau)$ and cross-correlation functions $R_{xy}(\tau)$ for random noise [(a) and (b)] and FM-TDS methods [(c) and (d)]. Modulation bandwidth: 0–200 Hz; sample: 400-μm quartz; Time-delay parameters were as follows: (a) $\tau_d = 35.2$ ms and $\Delta\tau_d = 30$ ms; (b) $\tau_d = 35.2$ ms and $\Delta\tau_d = 29$ ms; (c) $\tau_d = 35.2$ ms and $\Delta\tau_d = 30$ ms; (d) $\tau_d = 35.2$ ms; $\Delta\tau_d = 25$ ms.

The primary variables affecting the quality of an FM-TDS measurement are the sweep rate and frequency span, since they directly affect the uniformity of the input autospectrum according to Eqs. (15) and (16). Increasing the sweep rate affects the swept wave measurement in three ways: (1) by increasing the cross terms $R_{x_+x_-}(\tau) + R_{x_-x_+}(\tau)$ in Eq. (16) or reducing the approximation of $R_{x_+x_+}(\tau) + R_{x_-x_-}(\tau)$ to the IFT of the square frequency window. The result in both cases is a poor approximation of $R_{xx}(\tau)$ to a delta function; (2) by introducing nonlinearities into the system response. This occurs when the sweep time T is less than the longest delay components in the photothermal system[4]; and (3) by decreasing the effective frequency resolution of the sweep so that narrow resonances in the system response are missed, i.e., not resolved.

In the present experiments, the sweep rate S was adjusted by increasing the modulation bandwidth of the sweep. The increase in Δf, in the HP 3562A system, resulted in a concommitant decrease in the sweep time due to the instrumental requirement of constant data point resolution (2048 points). The product of the sweep time T and the modulation bandwidth Δf was maintained constant at $(\Delta f)T = 800$, in the linear resolution measurement mode.[15] Under these conditions, the effect of errors in $R_{xx}(\tau)$ by the cross-term contribution [Eq. (16)] is maintained constant because, for sweeps which include the dc level ($f_a = 0$), their contribution is approximately $1/[8\sqrt{(\Delta f)T}]$, with the product in the denominator maintained constant by the analyzer. Any sweep rate effects on $h(\tau)$, under this condition, are due to either errors in the approximation: $R_{xx}(\tau) \approx R_{x_+x_+}(\tau) + R_{x_-x_-}(\tau) = \delta(\tau)$, or to the effects of nonlinearities in the photothermal system response, or underresolution of narrow spectral features. The effect of increasing S on $h(\tau)$ [with constant $(\Delta f)T$] is shown in Fig. 6 for the PVF_2 detector film and for a thin sample of glass (500 μm). These results indicate that the only effects of increasing S in the range of modulation bandwidths from 0–25 Hz to 0–1 kHz is to vary the time-delay resolution of the recovered impulse response. There is no time-delay distortion of $h(\tau)$ as a function of sweep rate from 981 mHz/s to 5 kHz/s indicating the absence of nonlinearities in the output response of the photopyroelectric system, at least over the signal range related to thermal transit times. The effect of underresolution of sharp-frequency-domain resonances is clearly not observed here because signal resolution improves with increasing sweep rate, the sole factor affecting time-delay resolution being the modulation bandwidth Δf.

If the frequency span is too narrow, large errors are introduced into the impulse response peak delay, i.e., the result

Downloaded 18 Jul 2008 to 128.100.49.17. Redistribution subject to AIP license or copyright; see http://rsi.aip.org/rsi/copyright.jsp

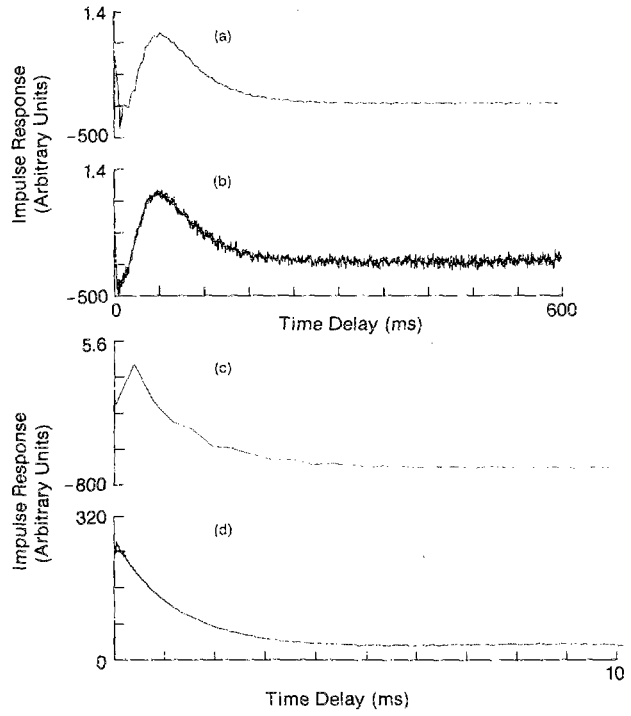

FIG. 6. Effect of sweep rate on recovered $h(\tau)$ for [(a) and (b)] 500-μm quartz sample and [(c) and (d)] thin-film PVDF using FM-TDS excitation. Time-delay and sweep parameters were: (a) $\Delta f = 0$–50 Hz, $\tau_d = 62.5$ ms, $\Delta\tau_d = 50.8$ ms; (b) $\Delta f = 0$–1 kHz, $\tau_d = 62.5$ ms, $\Delta\tau_d = 48.0$ ms; (c) $\Delta f = 0$–1 kHz, $\tau_d = 390$ μs, $\Delta\tau_d = 976.5$ μs; (d) $\Delta f = 0$–25 kHz, $\tau_d = 62.5$ μs, $\Delta\tau_d = 843.75$ μs.

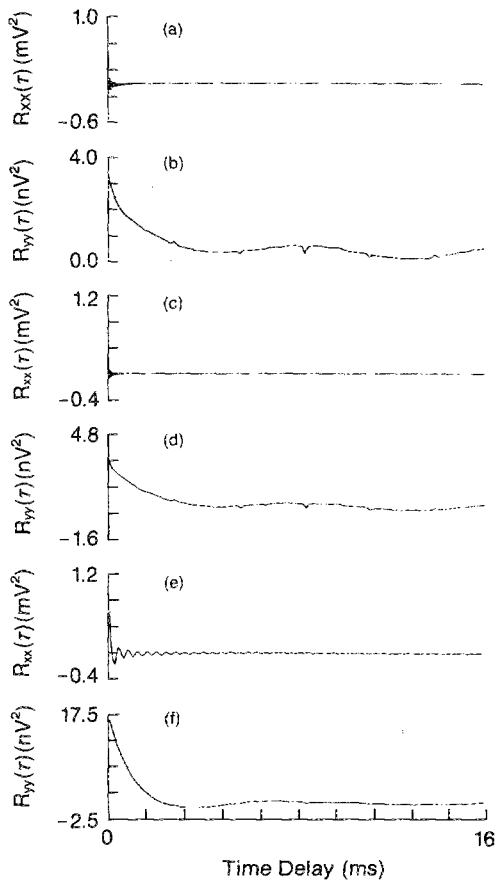

FIG. 7. Input/output autocorrelation functions for thin-film PVDF detector excited by FM-TDS (a), (b), (e), (f) and random noise (c), (d) waveforms; (a) $R_{xx}(\tau)$ and (b) $R_{yy}(\tau)$ for random excitation with $\Delta f = 0$–25 kHz; and [(e) and (f)] FM-TDS excitation with $\Delta f = 0$–5 kHz. Each recording was the result of 300 averages.

is an insufficient range of Fourier components to successfully reproduce the thermal transit time information contained in the impulse response. Distortions of the signal information due to limited Δf did not contribute to the results reported in Figs. 6(a) and 6(b) for the 500-μm glass sample, since most of the information for this material was centered at very low frequencies. The effects of Δf on the PVDF detector film [Figs. 6(c) and 6(d)], by comparison, were quite pronounced. The lower-frequency span ($\Delta f = 0$–1 kHz) was incapable of accurately resolving the rise time of the PVDF detector since significant high-frequency Fourier components corresponding to the early rise-time features were not included in the sweep. Increasing the frequency span to 25 kHz enabled the resolution of the detector rise-time [Fig. 6(d)] signal components.

An additional criterion for the success of a wideband-modulation experiment is the relative width of $R_{xx}(\tau)$ in comparison with $R_{yy}(\tau)$. Experimentally, we require the condition that $R_{xx}(\tau)$ be much narrower than $R_{yy}(\tau)$ for a given measurement. This comparison is made for both methods in Fig. 7, for the PVDF thin-film detector, which sets the upper limit on the frequency-modulation bandwidth required in these experiments. The information in Figs. 7(c) and 7(d) was recovered from excitation with a modulation bandwidth, $\Delta f = 5$ kHz. The approximation to a Dirac delta function is limited by the value of Δf. Increasing the frequency span to 25 kHz results in a better resolution of the film response, although resolutions this high were usually not required for the sample thicknesses of interest in these experiments[5] (Fig. 7). For thicker samples ($l = 500$-μm glass for example), a much lower Δf was required to maintain this condition (Fig. 8).

The quality of the Dirac delta functions available as $R_{xx}(\tau)$, in these experiments, is similar for both FM-TDS and pseudorandom methods, yielding short-pulse equivalents limited in resolution only by the modulation bandwidth of the excitation. Due to the details of the autospectral density flatness $G_{xx}(f)$, there were, however, slight differences in the degree of narrowness of $R_{xx}(\tau)$. For FM-TDS excitation, the autocorrelation peak was just slightly wider than the random noise estimate of $R_{xx}(\tau)$ with both delta functions lying effectively at the band limit of the excitation. This part is addressed in detail in the next section. The random noise excitation used in these experiments, in contrast with the PRBS waveforms that have often been used in photoacoustic and photothermal deflection spectroscopy,[7,12,17,18] bears a close resemblance to true random signals. Random noise excitation records, $x(t)$ averaged over time, were shown to decay in amplitude by a factor of nearly $\sqrt{N}$, where N is the number of averages, as is typical of time profiles whose amplitudes are governed by a Gaussian probability distribution.[14] The PRBS waveform contains components that appear random only within a single measurement

Downloaded 18 Jul 2008 to 128.100.49.17. Redistribution subject to AIP license or copyright; see http://rsi.aip.org/rsi/copyright.jsp

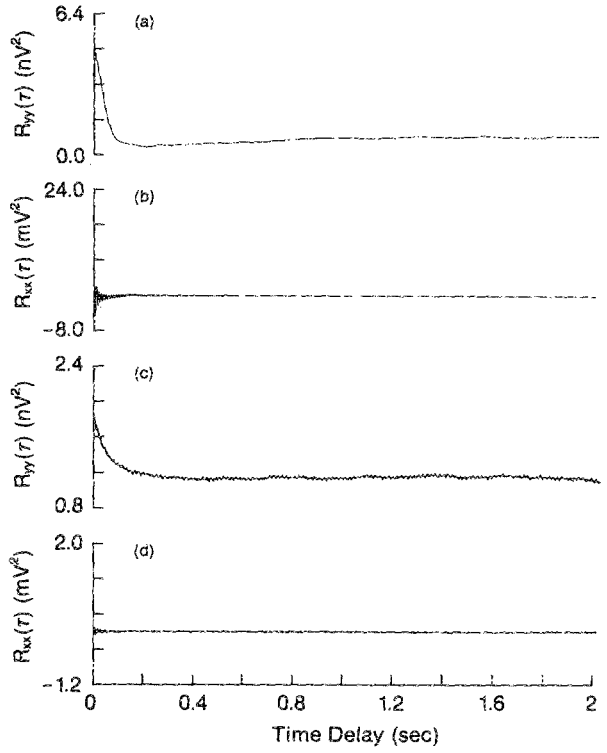

FIG. 8. Input/output autocorrelation functions for 400-μm quartz sample with $\Delta f = 0$–200 Hz. (a) $R_{yy}(\tau)$ and (b) $R_{xx}(\tau)$ for FM-TDS excitation; (c) $R_{yy}(\tau)$ and (d) $R_{xx}(\tau)$ for random noise excitation.

record, but which are repeated periodically over accumulated records. Previous work by Mandelis *et al.*[7] made a comparison of the FM-TDS and PRBS methods in photothermal deflection spectroscopy. The problems associated with the PRBS waveform were (a) frequency resolution limited by the number of elements used in synthesizing the PRBS waveform; and (b) leakage of higher harmonics of the fundamental repetition frequency of the PRBS waveform. The first effect, (a), produced broadened $R_{xx}(\tau)$ and $R_{yy}(\tau)$ values relative to the FM-TDS results. The second effect, (b), produced secondary signal maxima, displaced from the main responses, in $R_{xx}(\tau)$ and $R_{xy}(\tau)$. In the present experiments, the random noise signal is essentially aperiodic, relative to the measurement time scale of individual records. Therefore, leakage to higher harmonics is eliminated. The problem of limited source resolution is also eliminated since the frequency resolution in these experiments is limited by the user-selected modulation bandwidth, Δf, and the analyzer's record length (2048 points in the linear resolution mode[15]) rather than by the waveform synthesis limitations of the PRBS technique.

B. Frequency-domain system performance

In conventional cw photopyroelectric experiments the method of data presentation has usually been via the frequency domain, since lock-in measurements directly yield the frequency response of the photothermal system. Lock-in measurements, being too time consuming, generally lack the resolution to yield high-fidelity impulse-response information (by inverse Fourier transformation of the experimental data). The frequency-domain representation is generally not as easily interpreted as the impulse response, since the latter is theoretically modeled via the Green's function for the photothermal system,[5,6] while the former is the result of time-multiplexed information at a given response frequency of a system.

In cw broadband-modulation experiments, there is no experimental reason to prefer frequency over time-delay representations (or vice versa) since both are obtained via FFT methods. In fact, the information obtained from the two domains is complementary. The time-delay-domain impulse response gives the more direct visualization or the physics of the evolution of a photothermal system, because it yields time-resolved thermal transit time information. This information is, in principle, available in the phase channel of the frequency response. In practice, however, it is harder to extract from the frequency domain than from the impulse response data due to contributions from many time-multiplexed sources to the former. The impulse response also gives the experimenter a more direct diagnosis of nonidealities in the photothermal (or in this case photopyroelectric) system itself since problems such as contact resistance between the sample and detector, or stray detector response (caused by light leakage onto the PVDF film) show up very recognizably in the time delay domain and less so in the frequency domain. The frequency domain, on the other hand, gives a much more sensitive evaluation of the quality of the system response, dynamic range, SNR distribution, and overall instrumental performance.

An advantage provided by frequency-domain measurements is that they may be experimentally standardized against the single-point measurements made with lock-in amplifiers. The HP 3562A FFT analyzer contains a slow-sweep measurement setup which enables point-by-point frequency domain measurements to be made. Initial experiments demonstrated agreement between the frequency response data obtained by these slow sine measurements and results obtained with lock-in amplification. Consequently, the slow sine measurements made with our HP system were used as a standard representation of the "true" frequency response of the photopyroelectric system. It should be emphasized that the excitation obtained in the slow sweep mode was not equivalent to FM-TDS linear sweep excitation. In the slow sine mode, the frequency-domain functions were evaluated on a point-by-point basis using narrowband Fourier integration of a predetermined number of cycles of each frequency component in the sweep. The FM-TDS measurement involved broadband excitation and recovery of information via the cross and power spectral density measurements outlined in Eqs. (3)–(6).

The first test of signal quality was to compare measurements made with FM-TDS and random noise waveforms standardized against the data obtained from slow sine sweeps. Figure 9 makes this comparison for $H(f)$ of the thin-film PVDF detector as recovered by (a) slow sine (point by point) sweeps, (b) FM-TDS modulation, and (c) random noise excitation. The responses obtained from the latter two measurements were congruent with the slow sine

Downloaded 18 Jul 2008 to 128.100.49.17. Redistribution subject to AIP license or copyright; see http://rsi.aip.org/rsi/copyright.jsp

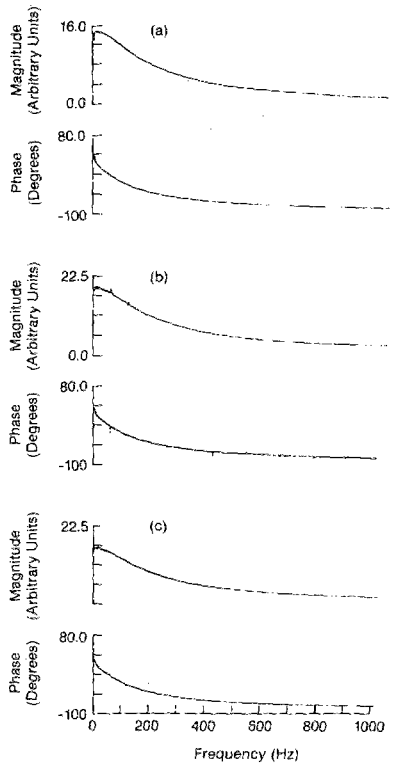

FIG. 9. Frequency-response (transfer function) data (magnitude and phase) for thin-film PVDF detector measured with $\Delta f = 0$–1 kHz (a) slow sine (lock-in equivalent) recording; sweep rate = 2.74 Hz/s, (b) FM-TDS excitation: sweep rate: 1.25×10^3 Hz/s; (c) random noise recording; (b) and (c) are the result of 100 averages.

measurements after a sufficient number of averages, indicating that the recovered $H(f)$ corresponded to the "true" frequency response of the PVDF element. In the case of the FM-TDS measurement [Fig. 9(b)], high-quality $H(f)$ data were also available. However, FM-TDS excitation, as expected,[15] was more sensitive to nonlinearities in our spectrometer system, the most important nonlinearity in our apparatus being the response of the acousto-optic modulator, which showed significant harmonic distortion at moderate input levels. Distortions in the photopyroelectric frequency responses recovered by FM-TDS excitation were directly traceable to distortions in $x(t)$ arising from modulator harmonic content. The distortions increased directly with the $x(t)$ drive voltage applied to the modulator input and were effectively eliminated at levels of 100 mV (peak to peak) or less, yielding the frequency responses of Fig. 9(b). The disadvantage of this compromise is the drop in modulation depth produced with low applied voltages. The random noise measurements [Fig. 9(c)] were less susceptible to any nonlinear effects because the P^2E system was excited differently for each data record, and the harmonic contributions averaged to zero.[15] In the case of the slow sine recordings, harmonics were not detected because of the narrowband Fourier integration used in the signal recovery. It should be emphasized that these harmonics are, in fact, distortions in the excitation wave train, rather than true system response-related nonlinearities. The modulator distortions were found to produce ripple in both $H(f)$, $G_{xy}(f)$, and $G_{xx}(f)$ for recordings made using a beam splitter and photodiode, which directly sampled the modulated Ar^+ ion laser beam intensity and applied this signal to the analyzer as $x(t)$. The effect of these nonlinearities, while severe in the frequency domain, had a very minor effect on the quality of the recovered impulse response information: $h(\tau)$ values obtained from FM-TDS measurements matched results obtained with random noise excitation to within experimental error over the time-delay-domain region corresponding to the thermal transit time information. This agreement was observed even at $x(t)$ levels where the distortions were present.

The critical factor affecting the quality of the frequency-response information available in a broadband-modulation experiment is the flatness of the input autospectrum $G_{xx}(f)$. In practice, the flatness of $G_{xx}(f)$ is limited by the frequency span Δf and by windowing effects which further reduce the width of the excitation spectrum within the span.

A problem generally associated with wideband excitation techniques is the problem of leakage due to signal components which are not periodic in the time record. The problem is normally corrected by imposing a time window on the data records to suppress signal amplitudes at the edges of the time records. We have found, in practice, that leakage appears to make a very minor contribution to the recovered photothermal signals in the time-delay regimes accessed by this work (100 μs to 1 s). This observation applied to both random and FM-TDS measurements.

Spectral flatness is examined in Fig. 10, which compares $G_{xx}(f)$ and $G_{yy}(f)$ with random noise and FM-TDS excitation for the PVDF detector element using a fixed modula-

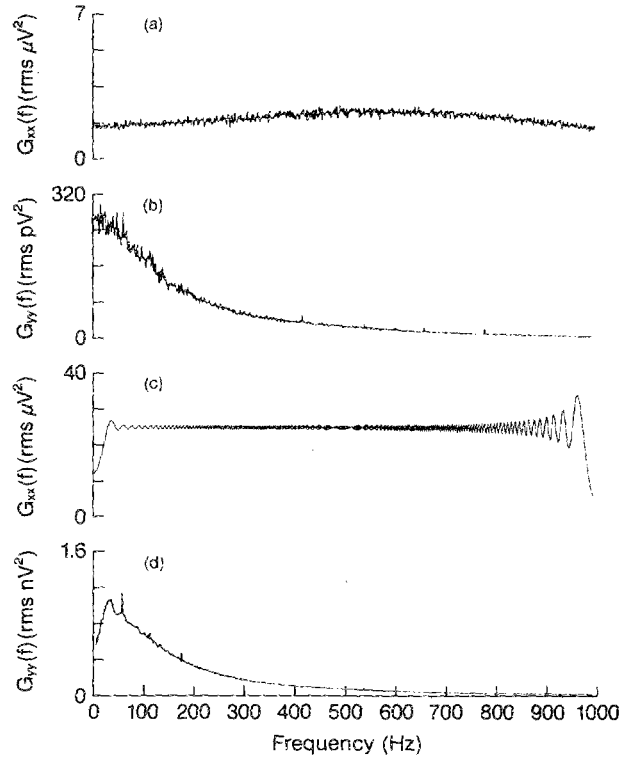

FIG. 10. Input and output autospectral density functions for thin-film PVDF detector and $\Delta f = 0$–1 kHz. (a) $G_{xx}(f)$ and (b) $G_{yy}(f)$ for random excitation; (c) $G_{xx}(f)$ and (d) $G_{yy}(f)$ for FM-TDS excitation.

Downloaded 18 Jul 2008 to 128.100.49.17. Redistribution subject to AIP license or copyright; see http://rsi.aip.org/rsi/copyright.jsp

tion bandwidth of 1 kHz. The random noise measurement showed some curvature in the autospectrum over the entire frequency span with a gently sloping power increase towards the midband ($\leqslant 30\%$). The FM-TDS measurement, by contrast, is nearly flat over the effective midband with sharp power losses ($\sim 50\%$) near the edges of the span. The average power of the FM-TDS waveform was consistently higher than that of the random waveform for equivalent signal levels due to the higher rms/peak ratio for the FM-TDS excitation. The result is a higher SNR for the FM-TDS system compared with the stochastic system. The power losses at the low-frequency edge of the span are responsible for the distortions in $R_{xy}(\tau)$ relative to $h(\tau)$ as seen in the previous section (Fig. 5). In general, the distortions in $R_{xy}(\tau)$ are present at time delays corresponding to the lowest and highest frequencies in the span under Fourier transformation. The drop in power explains the lack of agreement in $\Delta\tau$ observed for $R_{xy}(\tau)$ and $h(\tau)$ (Fig. 5). The problem is essentially absent in random noise experiments since the excitation power is more uniformly distributed over the entire span.

The effect of power losses and nonuniformities at the upper end of the span has an effect on the width of the input autocorrelation function (i.e., the impulse), $R_{xx}(\tau)$ recovered from $G_{xx}(f)$. Impulse functions $R_{xx}(\tau)$ recovered from random noise excitation decayed to the baseline at times t equal to $1/(2.56 f_{\max})$ where $f_{\max}$ is the upper end of the frequency span. Consequently, the impulse functions lay within a band limit set just above the aliasing frequency at $2.56 f_{\max}$. The impulses recovered by FM-TDS excitation, by contrast, were slightly wider, crossing the zero axis of $R_{xx}(\tau)$ at times approximately equal to $1/f_{\max}$, so that the effective band limit was set by the maximum frequency in the span. The difference in the two peak widths may be attributed to the differences in the flatness of $G_{xx}(f)$ at the upper edge of the span. Both methods, however, produce delta functions which are (nominally) span limited.

In spite of errors introduced in $R_{xy}(\tau)$ relative to $h(\tau)$ for FM-TDS excitation, the power losses at the edges of Δf are not sufficient to introduce significant errors in $H(f)$ relative to random noise measurements, as seen from the data of Fig. 9 (although a power loss of 50% seems larger, this corresponds to a loss of excitation amplitude of about 30% because of the square root relationship between amplitude and power). The flatness of $G_{xx}(f)$ is completely adequate to yield undistorted $H(f)$ and $h(\tau)$ recordings. This situation may be contrasted with other types of frequency-multiplexing techniques, such as the ac square wave excitation method reported by Coufal.[9] The use of excitation waveforms with narrow spectral power distributions was shown to drastically affect the dynamic range of the $H(f)$ measurement. A comparison of ac square wave with random noise excitation, also reported in that work demonstrated a greatly improved dynamic range resulting from the wideband character of the random noise excitation. In the present work, by contrast, the level of variation in $G_{xx}(f)$ between FM-TDS and random noise excitation is not sufficient to produce significant differences in the measured frequency-response-function quality.

C. Coherence and signal-to-noise ratios

The nature of the signals obtained in typical photopyroelectric experiments presents some important considerations in the choice of key experimental parameters such as Δf and S. Because of the diffusive nature of thermal waves, the frequency spectra of photopyroelectric signals are heavily weighted towards the lowest frequencies. The range of frequencies which correspond to the transit times of thermal signals through the PVDF film, however, generally lies well above the low-frequency range. The information which is of interest in the corresponding time-delay domain tends to be buried by the larger-magnitude low-frequency signal components. These low-frequency components yield information which corresponds to long time-scale heat conduction through the film and backing material under inverse Fourier transformation.

The diffusive nature of thermal wave information thus presents a problem for experimental design in that most of the information in $H(f)$ is centered at the lowest frequencies so that to optimize frequency resolution is to drastically reduce the time-delay resolution of the measurement with a loss of precision in the peak-delay and peak-width information. In order to better resolve both of these parameters, it is necessary to widen the frequency span Δf to include the extra frequencies carrying this information. The effect of increasing Δf, however, is to increase the noise level in $h(\tau)$ because the high-frequency components included in the measurement generally have poorer coherence than the lower frequencies. The measure of coherence between input and output signals is given by the ratio $\gamma^2(f)$, the coherence function, which is defined as[14]

$$\gamma^2(f) = \left(\frac{|H(f)|^2_{(\text{cross})}}{|H(f)|^2_{(\text{auto})}}\right) = \frac{|G_{xy}|^2}{G_{xx}G_{yy}}, \tag{19}$$

and measures the ratio between the magnitude of the frequency response computed from a cross-correlation measurement, Eq. (7), with that obtained from an autocorrelation measurement, Eq. (8). Since $|H(f)|_{\text{cross}} < |H(f)|_{\text{auto}}$, the ratio is always less than or equal to unity, with $\gamma^2(f) = 1$ representing perfect coherence. The coherence function is the most sensitive and direct measure of the quality of the relation between input and output signals. Because it is a direct indicator of the effective SNR distribution in the frequency domain, it provides an indicator of the frequency-response quality, and therefore, measurement dynamic range.

Figure 11 makes a comparison of the coherence functions available from our thin-film PVDF detector at frequency spans of 0–10 kHz and 0–100 kHz for (a) random noise and (b) FM-TDS excitation wave trains. The mean amplitude of both $x(t)$ wave trains was adjusted to a level of 200 mV peak to peak. Integration of $G_{xx}(f)$ for the random noise wave train gives a total power of 27.6 mV^2 compared with 38.5 mV^2 for FM-TDS excitation. This results from the superior rms/peak ratio for the FM-TDS excitation. The coherence functions recorded at 0–10 kHz [Figs. 11(a) and 11(b)] show only minor differences between the two methods, with excellent coherence observed in both cases

Downloaded 18 Jul 2008 to 128.100.49.17. Redistribution subject to AIP license or copyright; see http://rsi.aip.org/rsi/copyright.jsp

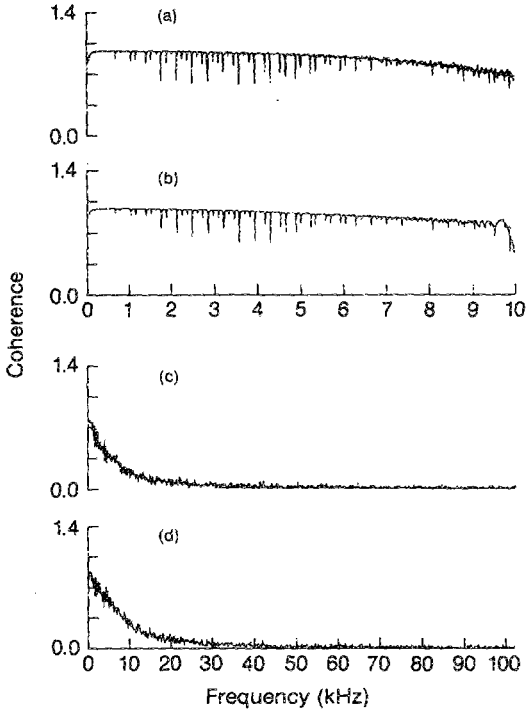

FIG. 11. Coherence functions recorded for random noise [(b) and (d)] and FM-TDS [(a) and (c)] methods. (a) and (b); $\Delta = 0$–10 kHz; (c), (d) $\Delta f = 0$–100 kHz.

$[\gamma^2(f) \sim 1$ over most of the signal range]. The sharp dips in the coherence function are due to nonsystem-related signal sources and are deterministic.[14] At the higher-frequency spans, where the PVDF signal is significantly attenuated (due to the diffusive nature of the thermal response), the coherence of the FM-TDS method was somewhat better than for the random noise technique, pointing to an improved dynamic range for FM-TDS. Instrumental factors cannot be completely discounted, however, because of the real-time bandwidth limitations of our FFT analysis system in this regime.

The improved rms/peak ratio for the FM-TDS technique does not entirely account for its SNR advantage over random excitation methods, however. A major advantage of FM-TDS is excitation by a deterministic waveform. Repeated frequency sweeps and response functions may be averaged over time to reduce noise by a factor of $1/\sqrt{N}$ where N is the number of sweeps averaged. The $1/\sqrt{N}$ reduction factor applies generally to random signals[14] with Gaussian probability distributions. In the case of random excitation where both $x(t)$ and $y(t)$ (input and response waveforms) obey the normal probability distribution, successive averaging of time records causes attenuation of the signal-related information as well as the "noise" by $1/\sqrt{N}$. In the case of an FM-TDS linear frequency sweep, the only random components present are due to extraneous noise: the noise contribution can therefore be arbitrarily suppressed by time averaging a sufficiently large number of FM-TDS *time* records. Therefore, if we consider the FM-TDS time records $x(t)$ and $y(t)$ (containing signal and noise), after a sufficient number of time averages, we obtain $\bar{x}(t)$ and $\bar{y}(t)$ in which the noise contributions are largely suppressed. The spectral functions $G_{xx}(f)$, $G_{yy}(f)$, and $G_{xy}(f)$, corresponding to the $x(t)$ and $y(t)$ records, contain the contributions of all Fourier components of x and y, signal and noise included. According to the Weiner–Khinchine relations of Eqs. (1)–(3), a true estimate of these spectral density functions is only arrived at after a sufficient number of averages in the frequency domain.

In theory, then, an infinite number of frequency-domain averages is required to yield true estimates of $G_{xx}(f)$, $G_{yy}(f)$ and $G_{xy}(f)$. The number of frequency domain averages does not improve SNR. It can only give a better estimate of the signal and noise power density inherently present in $x(t)$ and $y(t)$.

For the $\bar{x}(t)$ and $\bar{y}(t)$, time-averaged waveforms, the computed spectral density functions are $G_{\bar{x}\bar{x}}(t)$,$G_{\bar{y}\bar{y}}(t)$ and $G_{\bar{x}\bar{y}}(t)$. These functions contain few or no contributions due to extraneous noise because time averaging removed the noise from the time-domain records from which these functions were computed. The consequence is that the coherence of the FM-TDS excitation method may be arbitrarily improved with sufficient averaging of $x(t)$ and $y(t)$ time records.

In order to demonstrate the arbitrary coherence improvements available by use of FM-TDS, a series of measurements of $\gamma^2(f)$ was made for the PVDF detector at $\Delta f = 0$–100 kHz. The $x(t)$ amplitude was reduced by a factor of 10 in order to deliberately degrade the output response. The coherence of the FM-TDS signal was recorded for $N = 10$ averages in the frequency domain and is reported in Fig. 12(a). Signal coherence in this case is nearly zero, and corresponds to the "true" system coherence in the presence of background noise. A comparison was then made with FM-TDS measurements that had been recovered from time-averaged waveforms. In the second case, $N = 300$ averages were made for each time-averaged waveform $\bar{x}(t)$ and $\bar{y}(t)$. Ten data sets $\bar{x}(t)$ and $\bar{y}(t)$ were recovered, the spectral density functions were computed for each $\bar{x}(t)$ and $\bar{y}(t)$ pair, and the coherence function was computed for the ten sets by

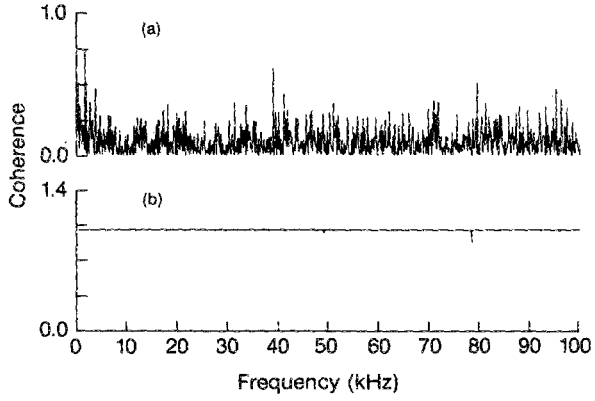

FIG. 12. Coherence improvement obtained with time averaging of FM-TDS waveforms. (a) Coherence obtained without time averaging, (b) coherence obtained with time-averaged data sets; $\Delta f = 0$–100 kHz.

Downloaded 18 Jul 2008 to 128.100.49.17. Redistribution subject to AIP license or copyright; see http://rsi.aip.org/rsi/copyright.jsp

the analyzer. The "time-averaged" coherence $\bar{\gamma}^2$ function, which has the form $(f) = |G_{\bar{x}\bar{y}}(f)|^2 / G_{\bar{x}\bar{x}}(f) G_{\bar{y}\bar{y}}(f)$ is reported in Fig. 12(b). The "time-averaged" coherence $\bar{\gamma}^2(f)$ is unity, from 0–100 kHz, indicating effectively perfect coherence. The result illustrates the great potential for signal quality improvement available from FM-TDS, and, in some cases, dynamic range and time-resolution improvement, since high-frequency components, which are normally quite attenuated in photothermal systems, may be recovered from extraneous noise.

It may be argued that this same SNR improvement may be achieved equally from pseudorandom techniques since the principle of noise reduction applies to the acquisition of any deterministic waveform with a well-synchronized trigger. Any improvement in signal quality over FM-TDS would be lost with pseudorandom binary sequence (PRBS) techniques, because of their relatively limited dynamic range.[7] The use of pseudorandom excitation, with an improved waveform synthesis, on the other hand, could perhaps yield results of comparable quality to the FM-TDS measurements reported here.

ACKNOWLEDGMENTS

The authors wish to acknowledge the partial financial support of the Natural Sciences and Engineering Research Council of Canada (NSERC) through an operating and an equipment grant. They also wish to acknowledge the partial support of the Ministry of Energy, Mines and Resources (EMR) through a grant to the Center for Hydrogen and Electrochemical Studies (CHES) throughout the work accomplished in all three parts of this report.

[1]H. Biering and O. Z. Pedersen, Bruel & Kjaer Tech. Rev. **1**, 5 (1983).
[2]H. Biering and O. Z. Pedersen, Bruel & Kjaer Tech. Rev. **1**, 43 (1983).
[3]R. C. Heyser, J. Audio Eng. Soc. **15**, 370 (1967).
[4]A. Mandelis, Rev. Sci. Instrum. **57**, 617 (1986).
[5]J. F. Power and A. Mandelis, Rev. Sci. Instrum. **58**, 2024 (1987).
[6]A. Mandelis, L. M. L. Borm, J. Tiessinga, Rev. Sci. Instrum. **57**, 622 (1986).
[7]A. Mandelis, L. M. L. Borm, J. Tiessinga, Rev. Sci. Instrum. **57**, 630 (1986).
[8]A. Mandelis, Chem. Phys. Lett. **108**, 388 (1984).
[9]H. Coufal, J. Photoacoust. **1**, 413 (1983–84).
[10]H. Coufal and P. Hefferle, Appl. Phys. **A38**, 213 (1985).
[11]C. E. Yeack, R. L. Melcher, and S. S. Jha, J. Appl. Phys. **53**, 3947 (1982).
[12]G. F. Kirkbright and R. M. Miller, Anal. Chem. **55**, 502 (1983).
[13]T. Sawada and M. Kasai, in *Photoacoustic and Thermal Wave Phenomena in Semiconductors*, edited by A. Mandelis (North-Holland, New York, 1987), Chap. 1.
[14]J. S. Bendat and A. G. Piersol, in *Engineering Application of Correlation and Spectral Analysis* (Wiley, New York, 1980).
[15]Hewlett–Packard model 3562A Dynamic Signal Analyzer Operating Manual, Hewlett–Packard, Everett, WA, 1985, pp. 1–20.
[16]J. F. Power and A. Mandelis, Rev. Sci. Instrum. **58**, 2018 (1987).
[17]A. Mandelis, IEEE Trans. UFFC **UFFC-33**, 590 (1986).
[18]Y. Sugitani, A. Uejima, and K. Kato, J. Photoacoust. **1**, 217 (1982).

Downloaded 18 Jul 2008 to 128.100.49.17. Redistribution subject to AIP license or copyright; see http://rsi.aip.org/rsi/copyright.jsp